CRISPR-Cas9 Activated Graphene Biointerfaces for Capture and Real-Time Monitoring of Cell-Free DNA on a Microneedle Patch

Bin Yang
Fudan University
Xueen fang (fxech@fudan.edu.cn)
Fudan University
Jilie Kong
Fudan University

Article

Keywords: CRISPR-Cas9, Epstein-Barr virus cell-free DNA, Graphene biointerfaces, Microneedle array, Wearable device

Posted Date: May 14th, 2021

DOI: https://doi.org/10.21203/rs.3.rs-468739/v1

Version of Record: A version of this preprint was published at Nature Communications on July 9th, 2022.
See the published version at https://doi.org/10.1038/s41467-022-31740-3.

Abstract

Recent advances in biointerfaces have led to the development of wearable devices that can provide insights into personal health. As wearable modules, microneedles (MNs) can extract analytes of interest from interstitial fluid (ISF) in a minimally invasive fashion. However, some MNs are limited by their ability to perform high-effective extraction and real-time monitoring for macromolecule biomarkers simultaneously. Herein, we explored the synergetic effect of clustered regularly interspaced short palindromic repeats (CRISPR)-activated graphene biointerfaces, and reported an on-line CRISPR wearable microneedles patch for extraction and in vivo monitoring of Epstein-Barr virus cell-free DNA (EBV CfDNA) in ISF. This wearable system can orientally capture and directly quantify unamplified ISF CfDNA in vivo within 75 min, with anti-interference ability of 60%, and has good electrochemical stability within 3 days (RSD = 9.04%). The experimental results of immunodeficient mouse models shows the feasibility and practicability of this proposed method. This wearable patch holds great promise for long-term in vivo monitoring ISF CfDNA and could be used for early disease screening and prognosis.

1. Introduction

With the arrival of the third medical revolution, wearable technology has experienced great development in the practice of modern personalized medicine. It is expected that wearable technology can become more streamlined, provide flexibility, and be integrated into personal characteristics[1]. Wearable technology is a multidisciplinary subject that mainly includes soft materials, flexible batteries, wireless signal communication, and chem-biosensing, which have garnered great attention for their ability to provide in-depth medical diagnostics and facilitate personal health assessments[2]. Although most efforts have focused on the analysis of small molecules or electrolytes[3–7], the next generation of wearables aims for noninvasive or minimally invasive detection of macromolecular biomarkers (e.g., proteins or DNA) [2,4]. However, the greatest challenge for such wearables may be the effective extraction and real-time in vivo monitoring of these biomarkers.

Interstitial fluid (ISF) is an ideal candidate for wearable chem-biosensors[4]. ISF contains a variety of biomarkers (e.g., protein, cells, nucleic acids) that are closely related to its blood concentration[2]. As an important component of wearable devices, microneedles (MNs) have been applied to ISF extraction in a safe, painless, and efficient manner[8–10]. In our previous studies[11,12], we proposed hydrogel MN patches to extract DNA from ISF and then analyzed them with portable flexible electrochemical microfluidics. However, this approach was still an offline monitoring method and would not be competent to the application of integrated wearable devices in real-world use. Therefore, the development of an online wearable system that can perform both sample extraction and real-time monitoring would be very important and could significantly improve personal health management.

Clustered regularly interspaced short palindromic repeats (CRISPR) technology has attracted extensive attention for the rapid analysis of nucleic acids specifically and accurately due to its precise gene editing

ability under the guidance of programmable single guide RNA (sgRNA) or CRISPR RNA (CrRNA)[13,14]. Unlike zinc-finger nuclease and transcription activator-like effector nuclease technology, CRISPR uses CRISPR-associated (Cas) effectors to recognize and edit specific gene sites, providing a promising method for sequence-specific detection, such as HUDSON-SHERLOCK [15,16] and DETECTR[17]. Recently, various amplification-free analytical strategies based on CRISPR have been developed for nucleic acids[18–21]. Hajian et al. proposed a graphene field-effect transistor based on CRISPR-Cas9 for unamplified samples, with a detection limit of 1.7 fM[20]. Subsequently, Fozouni et al. constructed an enhanced amplification-free CRISPR-Cas13a platform with multiple CrRNAs for SARS-CoV-2 detection, with a higher sensitivity of 0.16 fM[21]. Amplification-free CRISPR methodology could provide an effective and simple method for online nucleic acid wearable devices.

In this study, we propose CRISPR-Cas9 activated graphene biointerfaces on conductive MNs and combine them with reverse iontophoresis for the extraction and real-time monitoring of nucleic acids from ISF. Owing to the synergetic effect of CRISPR-Cas9 and graphene biointerfaces, the CRISPR-based wearable system was employed for real-time monitoring of Epstein-Barr virus cell-free DNA (EBV CfDNA), a biomarker released from nasopharyngeal carcinoma (NPC)[22,23]. This system has potential application value for real-time monitoring and early diagnosis of CfDNA-derived diseases.

2. Results And Discussion

2.1 Components, principle, and properties of the online CRISPR wearable patch

Here, we demonstrated an online CRISPR-Cas9 activated wearable patch based on the synergetic effect of CRISPR technology and graphene biointerfaces, where conductive MNs and reverse iontophoresis were employed for efficient extraction and real-time monitoring of EBV CfDNA from ISF in a minimally invasive fashion. A promising development in the study is the specific, continuous and direct monitoring of unamplified target DNA without preamplification (e.g., PCR or HCR). The CRISPR-activated wearable system includes the following modules: a flexible substrate, namely, a modified PDMS membrane; EBV CfDNA enrichment control, namely, a printed carbon nanotube (CNT)-functionalized component; and real-time monitoring control, namely, a three-electrode prototype CRISPR-Cas9 MN system.

As shown in **Figure 1a**, to achieve real-time monitoring of target DNA, the proposed wearable platform is composed of a spray-printed functional flexible patch and three-electrode conductive MNs. First, the surface of the PDMS membrane was treated with plasma to increase the hydrophilicity of the membrane. Then, a hydrophilic membrane was

fabricated on the PDMS membrane via drop-casting of 1% chitosan solution. Due to the soft characteristics and weak surface adhesion of PDMS, the percolating microstructure would be deformed out of the interface during bending, stretching, and twisting[24]. Inspired by these properties, CNTs were deposited on the modified PDMS film by inkjet printing using a spray gun (0.17 MPa, 300 μm diameter) in this study[12]. The printed CNT pattern acted as a reverse iontophoresis compartment, separating negatively charged compounds (e.g., nucleic acids or ascorbate). Finally, a conductive CRISPR microneedle array as the working electrode was attached to the anode side of the CNT pattern. The CRISPR MNs showed three functions during real-time detection: (I) insertion into the epidermis to isolate and concentrate target DNA; (II) CRISPR gene editing specifically performed by Cas9/sgRNA immobilized on the surface of the CRISPR MNs; and (III) the formation of a three-electrode system to record electrical signals.

Figure 1b shows a scheme of CRISPR MNs construction. In this CRISPR-Cas system, we used a catalytically inactivated Cas9 enzyme (dCas9) to form Cas9/sgRNA, denoted as dRNP[25]. Although both nuclease domains (RuvC and HNH) are deactivated in dCas9, the dRNP retain the ability to bind specifically to target DNA[13, 26, 27]. Immobilized dRNP can scan the entire DNA sequence under the guidance of sgRNA, where a 20-nt specific sequence matches the target DNA[14]. Once matched, dRNP can unwind the double-stranded helix and specifically bind with target DNA directly upstream of the 5’-NGG protospacer adjacent motif (PAM). The real-time monitoring capability of the wearable patch may come from two aspects: (I) dRNP of CRISPR-Cas9 as a driving force continuously searched and recognized target DNA; and (II) graphene biointerfaces on MNs provided highly efficient charged compound interactions and electron transport. In **Figure 1c**, hybridization of dRNP on the surface of graphene with CRISPR gene editing targets not only altered the conductivity of the graphene interface channel but also resulted in counterion accumulation. Therefore, an ion-permeable layer was generated on the graphene surface to maintain charge neutrality. The difference in ion concentration between the bulk solution and the ion-permeable layer produced the Donnan potential[28]. Hence, the recorded output electrical signals can reflect the real-time recognition of the

target EBV CfDNA, and the theory and corresponding verification are deduced in the Supplementary Information (Supplementary note 1 and **Figure S1**).

2.2 Validation and affinity of dRNP to target DNA

To validate the feasibility of the CRISPR wearable system, we first tested the CRISPR-Cas9 reaction for EBV CfDNA gene editing in solution. From the genotyping data in **Figure 2a-2b**, two new bands in lane 1 were observed due to CRISPR gene editing, which contained Cas9, sgRNA and EBV CfDNA. Additionally, it was elucidated that the CRISPR reaction did not occur with mismatched sgRNA or sgRNA-free sequences. Accordingly, sgRNA plays an important role in the CRISPR-Cas system[14]. To this end, optimized experiments for sgRNA screening were performed in this study (Supplementary Information, **Figure S2**). The effect of the selected sgRNA on triggering CRISPR-Cas9 was verified in a concentration-independent manner, as shown in **Figure S2**. According to region of interest (ROI) analysis of the PAGE gel results, the average ROI value of the CRISPR product bands gradually increased, while that of EBV CfDNA decreased (**Figure S2**).

Then, we used a commercial solid microelectrode for EBV CfDNA target CRISPR gene editing on a skin chip (37 °C, pH 7.4). **Figure 2c** shows the original i-t curve data in response to 10^9 copies/μL EBV CfDNA. Compared with that of the control group, the fitting curve of EBV CfDNA was stable within 200 s and gradually increased after 400 s. The results showed that the current output signal comes from the directional recognition and binding of the target by the dRNP complex. In **Figure 2d**, there was a significant difference in the current between the positive and control groups, which was related to the appearance of the Donnan potential. These results might primarily demonstrate the proposed mechanism by which the dRNP compound immobilized on microneedles plays an important role in real-time online capture and monitoring of target DNA.

In this study, a CRISPR-Cas9 driving strategy was designed for wearable patches to monitor the CfDNA of ISF in real time. Therefore, the most important aspect is to ensure that dRNP has the ability to recognize and detect EBV CfDNA. For this purpose, we conducted experiments on a solid-state microelectrode (schematic in **Figure S3**). The targeting dRNP was modified on the surface of the microelectrode by a method similar to

that used to prepare conductive microneedles. The CV and EIS characterization results using 0.05 M $[Fe(CN)_6]^{3-/4-}$ as a probe confirmed the successful fabrication of the CRISPR microelectrode (**Figure 2e-2f**). In comparison to that of the bare microelectrode, the peak redox current of the modified microelectrode was decreased because the repulsive force between the probe and CRISPSR-Cas9 sensitive film hindered interface electron transfer.

To evaluate the specificity of CRISPSR-Cas9, conserved sequences of West Nile virus (WENV, GenBank NO. M12294.2), Japanese encephalitis virus (JPEV, GenBank NO. NC001437.1), and dengue virus (DENV, GenBank NO. AF326573.1) cloned into the PUC57 plasmid were chosen for interference (1×10^{-8} M). As shown in **Figure 2g**, compared with the detection of 1×10^{-10} M EBV CfDNA, the current intensities of the interference group did not change obviously and had higher significance (P= 0.001, 0.002, and 0.001 for WENV, JPEV, and DENV, respectively).

To explore the quantitative analysis and real-time ability of this method, the CRISPR microelectrode was applied to test variable concentrations of EBV CfDNA. According to reference[20], we used **Equation 1** as the unit of this real-time monitoring, where I response reflected the change between I_t (measurement after incubation) and I_b (calibration background before measurement).

$$I\ response(\%) = \frac{I_t - I_b}{I_b} \times 100\% \qquad (1)$$

In **Figure 2h**, the real-time monitoring plots could be divided into four regions: (I) region 1 (t<5 min), where the signal did not increase significantly and was basically in a fluctuating state; (II) region 2 (5 min<t<30 min), where the signal response of the positive sample increased drastically, but that of the NTC group did not change; (III) region 3 (t>30 min), where the signal of the positive groups tended to be stable, which might indicate that the CRISPR reaction on the interface reached adsorption equilibrium under reverse iontophoresis; and (IV) region 4 (simulating drug treatment, TE buffer under stirring, pH 8.0, 15 min, 37 °C), where some EBV CfDNA on the interface was eluted, and the signal response value decreased. However, the NTC group did not show a corresponding signal

response to these four processes. Similar to nucleic acid amplification (e.g., PCR) [29,30], we hypothesized that there might be a defined time threshold for this protocol. The derivative of the real-time I response was obtained in **Figure 2i**, that is, dI/dt and CRISPR reaction time. The time threshold of this experiment was defined as ~12 min. That is, if there was no obvious change in the I response curve after ~12 min, it could be judged to be a negative sample.

To test whether this assay was quantitative, we defined a signal threshold for varying concentrations of EBV CfDNA. According to the derivative curve, we found that there was no significant change after 30 min, which was chosen as the signal limit. In **Figure 2j**, within the signal threshold, a linear relationship was observed between the change in the I response and EBV CfDNA concentration (fM, C) in the range of 30 fM-30,000 fM following the equation Δ I response (%) = 30.8316·lgC+168.8204 (R=0.9736), with a detection limit of 1.1 fM (DL = $3\delta_b/K$). In addition, the end-point method and EIS dynamic curves further demonstrated the feasibility of this strategy, as shown in the Supplementary Information (**Figures S4-S7**). In particular, this kind of label-free biosensing strategy using hybrid nanomaterials with high carrier mobility, such as graphene[3] or CNTs[7], can mitigate charge shielding effects and sensitivity limitations. Herein, dRNP immobilized on graphene biointerfaces could be used to trigger the event of target DNA detection without reagents or bulky equipment.

The above results primarily illustrated that dRNP on the surface of the microelectrode can recognize and bind target DNA. We were also interested in the binding constant between dRNP and EBV CfDNA; therefore, UV-vis spectrophotometry was employed to verify the interaction between the two[11]. As seen from the data in **Figure 2k** and **2l**, the binding constant of K_b=1.02 × 10^7 L/mol indicated that there was a good interaction between dRNP and EBV CfDNA. These results suggested that CRISPR-Cas9 can be employed in the subsequent microneedle array to achieve real-time monitoring.

2.3 Characterization and evaluation of the CRISPR wearable patch

In this study, we first fabricated conductive MNs using a series of simple and general methods, including drop casting and ion sputtering. The detailed preparation and

optimization procedures are discussed in the Supplementary Information (**Figure S8**). From the results of **Figure S8**, we found that the rigidity and modulus of the microneedles was closely relative to its shapes and inertial distance. In addition, to test whether the graphene biointerfaces on the MN surface were rigid enough to perform the CRISPR reaction, we compared the membranes under different conditions by scanning electron microscopy (SEM) (Supplementary Information, **Figure S9**). **Figure 3a** showed an off-the-shelf MNs that can be used directly for CRISPR-Cas9 decoration and wearable application. As shown in **Table S1**, conductive MNs have been increasingly considered a promising tool for continuously monitoring from small molecules to biological macromolecules (e.g., RNA, DNA, protein), while it is still challenging to realize sample extraction and detection of nucleic acids simultaneously. In our research, reverse iontophoresis was used for preliminary enrichment and separation of the samples, which is an effective candidate for microneedles extraction function[12, 31]. On this basis, real-time monitoring was performed by conductive MNs.

To test the quality of the prepared MNs, cyclic voltammetry (CV) was performed using $[Fe(CN)_6]^{3-/4-}$ as a probe, as shown in **Figure 3b** and **3c**. From the data, it was observed that the area of the CV plot increased as the scanning rate increased. Two linear relationships between the scanning rate and redox peak current were obtained. The above results implied that the well-defined conductivity and mass transfer of the MNs was subject to a diffusion-limited mode[32]. Due to the high specific surface area, the prepared MNs outperformed a commercial gold electrode (GE, diameter of 2 mm) at a peak current of 1 mM $[Fe(CN)_6]^{3-/4-}$ probe (**Figure 3d**). One of the concerns was whether the MNs could be utilized for real-time i-t measurement. Therefore, we compared MNs with commercial GE in PBS buffer (0.01 M, pH 7.4) in **Figure 3e** and **3f** for real-time recording. Compared with commercial GE, MNs had reliable electrochemical performance and amplified the electrical signal by 6.5 times. Additionally, the stability of MNs was investigated by CV measurements in different periods of 3 days, with an RSD of 9.04% (n=9).

To construct the wearable patch, poly dimethylsiloxane (PDMS, Sylgard 184, Dow Corning) was chosen as a candidate substrate due to its elastic and stretchable properties.

However, it is generally believed that the interface of PDMS is somewhat hydrophobic, which limits its application in wearable chem-biosensors[33]. One ideal method was to obtain the hydrophilic surface of PDMS by using stretchable and conductive nanomaterials, such as CNTs. Based on our previous report[12], we first modified the PDMS surface primarily by plasma treatment and then drop-casted 1% chitosan solution. The wettability of PDMS was characterized via a water contact angle (WCA) meter. As shown in **Figure 3g**, the droplets on the modified PDMS film changed significantly within 60 s (row II), while those on the surface of the original PDMS film changed little (row I). Through five-point fitting of the droplet distribution, the WCA of the modified PDMS film changed from 73.9° to 34.8°, and that of the original PDMS film changed from 98.4° to 95.3°. These results indicated that the surface wettability of PDMS had been effectively improved, which was probably due to the high permeability and good hydrophilicity of chitosan.

In **Figure 3h** and **3i**, demonstration of a skin-interfaced CRISPR wearable patch that integrated a reverse iontophoresis module and MNs biosensor for real-time tracking of EBV CfDNA from ISF was shown. As shown in **Figure 3j**, to further test the practicability of the CNT printed wearable patch, a blue light-emitting diode (LED) was activated by the patterned conductive region. The external power supply was 6 V, which implied the good conductivity of the printed wearable material for subsequent experiments. The printed wearable patch exhibited stable electrical performance in the static (**Movies S1**) or moving state (**Movie S2**). The concept of representative wearable patches has been validated by a finite element analysis (FEA) simulation under different mechanical distortions, including stretching, twisting, and bending (**Figure 3k**). The theoretical maximum modulus of the elastic wearable device at 16% stretch is ~0.07 MPa, which is comparable to human skin (25-220 kPa)[34], indicating that it can be conformally mounted on the skin.

One ideal method to fabricate stretchable sensors has typically involved depositing CNTs on the surface of PDMS films[24,35]. It is commonly recognized that soft PDMS allows deformation of the percolating network microstructure during different mechanical distortions, which may lead to cracks on CNT membranes[36]. As presented in

Figure 3k, we further explored the morphology of CNT-printed PDMS using SEM to understand the relationship between the CNT percolating network and the deformation of the modified PDMS film. After stretching and twisting the substrate film, it was observed that the resulting fractures tended to be in the direction of deformation, resulting from uniaxial or biaxial distortions. The bending action induced wrinkles along the uniaxial direction. The results showed that CNTs deposited on the surface of PDMS were connected with each other, forming a percolating network, and the electron pathway was unblocked during the different deformation processes.

To verify the stretchability of the wearable patch, a series of mechanical property tests were carried out, as shown in **Figure 3l-3o**. The maximum elongation at break of the prepared patch reached 26.8% in the range of ~0.4 MPa. During a stretch-release test, hysteresis of the patch was clearly observed at 10% strain, which could be attributed to the multiple modification layers on the PDMS surface. Endurance tests confirmed that this wearable patch had good fatigue resistance, with a coefficient of variation of 17.6% in 100 cyclic strain tests. For stretchable electronic devices, the gauge factor (GF) is one of the most important parameters to evaluate the sensitivity of devices, as shown in **Equation 2** below[37].

$$GF = \frac{\Delta R/R_0}{\varepsilon} \quad (2)$$

$\Delta R/R_0$ and ε refer to the stress change and strain, respectively. The GF value of this patch reached 282.6 with a maximum strain of 26.8%. According to Euler-Bernoulli beam theory[38], the bending resistance is proportional to the cube of the film thickness. Briefly, a thinner film is more flexible to mount the skin. Thus, the thinner the film is, the more elastic it is against the skin. Therefore, the surface modification of PDMS by chitosan with a high modulus results in low tensile properties but high sensitivity. For stretchable electronics, it is challenging to consider the effects of GF and strain simultaneously. The stretchable patch in this study demonstrated its reliability in the real world, even when compared to reported state-of-the-art flexible devices, such as polyurethane-PDMS nanomesh (GF=46.3, strain≈75%)[39], nanofibril percolated PDMS

(GF=33, strain=50%)[40], and self-healable semiconducting polymer film (GF=5.75×10^5, strain=100%)[41].

2.4 In vitro extraction and real-time monitoring of EBV CfDNA using a CRISPR MN patch

The ultimate goal of the proposed real-time method was to realize proof-of-concept recognition of CfDNA on wearable MNs. It is essential to determine the anti-interference and sensitivity of this system. Thus, based on our previous report[12], we used a simple skin chip to simulate human skin (37 °C, 10 V of reverse iontophoresis) as an in vitro real-time monitoring setup for the performance evaluation. As mentioned above, original conductive MNs were obtained for subsequent decorations, as shown in **Figure 4a**. Importantly, dCas9 was covalently immobilized, allowing the nuclease to bind tightly to the graphene surface.

The anti-interference of the CRISPR MNs was tested for the detection of 3×10^{-12} M EBV CfDNA with different concentrations of fetal bovine serum (FBS) and control samples, including 0%, 10% and 60% FBS. The signal was recorded by i-t curve, as shown in **Figure 4b**. The CRISPR MNs generated a stable and well-defined current response with a relative standard deviation (RSD) of 2.49% under the interference of 10% FBS when compared to 0% FBS interference. Moreover, we observed that 60% FBS had an effect on the CRISPR MNs, and the RSD was 20.95%, but it still showed an "S" curve within 75 min. This capability could allow CRISPR MNs to be used for wearables in the real world.

We also investigated the real-time monitoring and sensitivity of the CRISPR MNs, as presented in **Figure 4c**. Under reverse iontophoresis on the skin chip, CRISPR MNs were applied for EBV CfDNA detection. In contrast to the NTC group, EBV CfDNA was recognized and bound by dRNP on the CRISPR MNs surface in the two positive groups, producing significant signal output. As the concentration of EBV CfDNA increased, the relative I response increased, which corresponded to the CRISPR microelectrode. From the result of i-t curves, we found that the signal tended to be stable within ~30 min, illustrating that the total monitoring time of 75 min is sufficient. The above results showed that the sensitivity was 3×10^{-14} M.

As seen from the results in **Figure 4d**, the positive groups had a time threshold when compared with the NTC group. Interestingly, the time threshold increased as the

concentration of the target DNA increased. This result can be attributed to the following reasons: (I) CV testing showed that MNs were controlled by the diffusion-limited mode (**Figure 3b** and **3c**), which might have an impact on the time threshold of the CRISPR reaction; and (II) based on reported research where the saturation of I response was used to quantify the target DNA concentration[20], we primarily speculated that this kind of non-amplified detection method without a cycle reaction could not quantify the target concentration by the time threshold only.

Based on the aforementioned experimental results and previous reports, the real-time monitoring capacity of this CRISPR MN patch might be attributed to synergetic effects: (I) graphene, due to its excellent electrical sensitivity to charged molecule interactions on its surface, has found great applications in flexible and scalable electronic devices[42]. This material acts as a channel between MNs and the epidermal microenvironment and is an ideal candidate to produce Donnan potential (Supplementary Note 1). (II) Programmable dRNP, which acted as the driving force, could automatically search the entire gene sequence of the nucleic acid in the sample without amplification until it matched the target sequence. Importantly, it exhibited high spatiotemporal resolution in short-lived off-target binding events (average <1 s)[43].

Table 1 summarized some state-of-the-art amplification-free CRISPR methods for analysis targets. As shown, an unamplified detection strategy has been considered as a universal tool for molecular diagnosis since programmable sgRNA or CrRNA can be designed for different genomic samples. However, compared with HUDSON-SHERLOCK [15,16] or DETECTR[17] (detection limit down to aM levels), these reported amplification-free methods (mostly ranging from pM to fM levels) without PCR or other isothermal nucleic acid amplifications have yet to exhibit considerable sensitivity for low-abundance biomolecule detection. In this study, our proposed CRISPR wearable device combining CRISPR MNs with stretchable electronics showed potential advantages for portable, miniaturized, and wearable point-of-care testing.

Table 1. Comparison of representative amplification-free CRISPR-Cas strategy.

Method	Target	LOD	Time	Equipment	Ref.
Combined CRISPR-Cas13a device	SARS-CoV-2 RNA	0.16 fM	~30 min	Smart mobile phone microscopy	[21]
CRISPR-chip	Bfp-transfected HEK293T cells	1.7 fM	~15 min	Graphene-modified field-effect transistor	[20]
CRISPR microfluidic	MiR-19b and miR-20a	10 pM	~9 min	Electrochemical microfluidic biosensor	[18]
Electrochemical CRISPR biosensor	Transforming growth factor β1	0.2 nM	~60 min	Aptamer-based electrode	[19]
CRISPR-Cas12a Sensors based on functional DNA activator	ATP and Na^+	0.21 μM for ATP; 0.1 mM for Na^+	~40 min	Microcentrifuge tube	[44]
CRISPR-Cas9-mediated SERS assay	*S. aureus*, *A. baumannii*, and *K. pneumoniae*	14.1 fM for *S. aureus*; 9.7 fM for *A. baumannii*, and 8.1 fM for *K. pneumoniae*	~30 min	Microcentrifuge tube	[45]
CRISPR-Cas13a-mediated naked-eye platform	MiR-17	500 fM	<1 h	Microcentrifuge tube	[46]
Label-free CRISPR-Cas9 Assay	Double-stranded DNA template	0.13 nM	~35 min	ICPMS	[47]
Enhanced CRISPR-Cas electrochemical sensor	Double-stranded DNA template	~pM	~40 min	Hairpin DNA-modified electrode	[48]
Wearable CRISPR-Cas9 patch	EBV CfDNA	1.1 fM	~30 min	Conductive microneedles	This work

2.5 Demonstration of the CRISPR MN wearable system in vivo

The experimental timeline of real-time monitoring of EBV CfDNA in vivo based on reverse iontophoresis and CRISPR MNs was demonstrated in **Figure 5a**. To further verify the feasibility of the real-time online platform for in vivo EBV CfDNA detection, a luciferase reporter gene (Luc) was inserted into CNE cell lines and then subcutaneously inoculated into 8-week-old female BALB/c nude mice for subsequent experiments. Detailed cell and

animal experiments were listed in experimental section (Supplementary Information). Then, the constructed CRISPR MNs integrated with reverse iontophoresis components (external voltage of 10 V) were employed in BALB/c nude mice.

In earlier studies[23], it was reported that NPC was asymptomatic at an early stage. However, in numerous subsequent reports[22], it was shown that NPC-related EBV CfDNA could be detected in NPC-positive patients. It has been proposed that EBV CfDNA was released by cell apoptosis and necrosis in patients with distant metastasis and localized diseases. Therefore, it is worthwhile to monitor circulating EBV CfDNA real time in an on-demand, minimally invasive and specific manner.

To avoid signal crossover, this CRISPR MN platform applied an intermittent measurement, similar to the GlucoWatch® biographer (Cygnus, Inc., Redwood City, CA, USA)[49], as shown in **Figure 5b**. In brief, a voltage of 10 V was applied to extract the target for 3 min by reverse iontophoresis in the first step. Then, reverse iontophoresis was stopped, and the biosensor which remained to be laminated on the epidermis was engined for collecting electrochemical signal. The signal of this biosensor at the corresponding region was recorded for 1 min. These two steps were repeated to achieve real-time CfDNA monitoring.

As seen from the data in **Figure 5c**, the signals of the CRISPR MNs method (I response of 82.39%) and bioimaging method (maximum of 72 a.u.) were vividly identical 2 h after inoculating CNE-Luc, while optical imaging was ineffective for target screening at the early stage. Subsequently, at the 8-h time point (I response of 145.48%), the abundance of EBV CfDNA in mice monitored by our method was higher than that at the 2-h time point. At the same time, the bioimaging signal increased to a high value (maximum of 127 a.u.), consistent with CRISPR MNs. Subsequently, at the 72-h time point, our method could still monitor EBV CfDNA in real time (I response of 90.65%), and the bioimaging signal also decreased (maximum of 82 a.u.), possibly due to the heterogeneity of CNE-Luc cell lines during the formation of nasopharyngeal carcinoma. From the results of 120 h, although the bioimaging signal continuously decreased, it was still able to effectively distinguish the positive group (I response of 25.44%) and NTC group (I response of 11.20%). It could be

concluded that EBV CfDNA was closely related to CNE-Luc cells. However, naked-eye visualization was unavailable for the first five days. This CRISPR MN platform can not only effectively monitor EBV CfDNA real time in vivo but also be used for the early screening of nasopharyngeal cancer tumors. To further test whether the real-time I response shown in **Figure 5c** was indeed true, we compared the slopes by differentiating the I response curves at various time points, as presented in **Figure 5d**. This comparison confirmed that the slopes were proportional to the intensity of the biological imaging signals, and there was still a significant difference between the 120-h time point and NTC groups. During the first 5 days, the CRISPR MN wearable system was able to record dynamic changes in target DNA levels in BALB/c nude mice, showing the same trend as the bioimaging method (**Figure 5e**). These results illustrated that this wearable system would be expected to be employed for real-time monitoring of target CfDNA.

Unlike traditional labs, a wearable device is exposed to an uncontrolled environment for a long time, which might pose a challenge in detection accuracy during continuous monitoring[2]. Therefore, we conducted four independent tests on 18-day CNE-Luc-bearing BALB/c nude mice to verify the accuracy of the CRISPR MNs (**Figure 5f**, **Figures S10-S11**). For the CRISPR MN platform, the procedure is shown in **Figure 5b**; for gold-standard PCR (kit provided by TIANGEN Co., Ltd., Beijing), the sampling blood was first treated by a commercial DNA extraction kit (provided by Sangon, Shanghai). Compared with PCR, CRISPR MNs ensured a reliable qualitative detection in mice, but their quantitative detection ability was not yet known.

3. Conclusion And Outlook

In summary, based on the synergetic effect of CRISPR-Cas9 and graphene biointerfaces, this study proposed an online wearable conductive MNs that performed high-effective extraction and real-time monitoring for NPC-derived CfDNA from ISF in vivo. This CRISPR-Cas9 activated wearable patch could continuously monitor cell-free DNA targets from ISF in vivo, with a detection limit of 1.1 fM ($3\delta_b/K$), with good electrochemical performance and stability within 3 days (RSD = 9.04%).

However, two major challenges still remain in terms of wearable devices: (I) due to the instability of the immobilized bioreceptor, the interface between the device and the active sensitive film fluctuates during the dynamic deformation process. Additionally, Joseph Wang et al. pointed out that the detection

accuracy of wearables would be affected by the interface effect during continuous operation[2]. Unlike traditional laboratories, wearables are often exposed to harsh conditions that affect the bioactivity of immobilized receptors. Usage of a hydrogel or chitosan layer on the top to protect the immobilized bioreceptor may account for this issue. (II) Regarding sensitivity, probably due to the lack of preamplification, the current version of an amplification-free strategy could not meet the requirements of highly sensitive DNA detection. As shown in Table 1, the optimized sensitivity proposed by Fozouni et al. reached 0.16 fM for SARS-CoV-2[21], and that of our proposed assay was 1.1 fM for target CfDNA, which was still unavailable for low-abundance biomarker analysis in particular practical applications (single copies/μL). Therefore, subsequent studies, including those on multiple Cas proteins, ordered mesoporous nanomaterials, precalibration processes, and metallic microneedle patches, should further endeavor to improve interfacial receptor immobilization and sensitivity to achieve detection of single-copy DNA of interest.

4. Methods

4.1 Synthesis of polymethyl vinyl ether-alt-maleic acid (PMVE/MA) hydrogel

The reagents were provided by Aladdin corporation (Shanghai). Briefly, first, 10 g of PMVE/MA was dissolved in 60 mL of ddH_2O and reflux-stirred for 24 hours at 80°C. After cooling, 6 g of polyethylene glycol (PEG, MW = 8000 Da) was added into the PMVE/MA solution for 12-hour reflux-stirring at 28°C.

4.2 Microneedles preparation

We designed the conceptual microneedle scheme, and a metallic wafer with a negative surface pattern was processed by Wuxi Guorui Electronic Technology Co., Ltd. (Wuxi, China). The metallic wafer was used to replicate the PDMS mould shape of the microneedle array (12×12 microneedles, microneedle base diameter 300 ± 10 μm, microneedle height 600 ± 50 μm, microneedle tip 30 ± 10 μm, microneedle interval distance 300 μm). To obtain the hydrogel-based microneedle patch, three-step replication processes were conducted in this study. First, the metallic wafer was ultrasonically cleaned with ddH_2O for 3 min and then dried in an oven (80°C). Surface hydrophobic treatment was performed for metallic wafers for 5 min. PDMS was prepared at a weight ratio of base to curing agent of 10:1 and poured into the wafer. This metallic wafer mould was vacuumed (600 mmHg, 25°C, 30 min) to remove air from the PDMS matrix and centrifuged for 30 min (4000 rpm), which was repeated three times. Afterwards, this metallic wafer was placed in an oven (80°C, 4 h). The first replication of the PDMS microneedle patch was carefully peeled from the metallic wafer. Next, Ecoflex (smooth-on 0030) precursor mixture at a weight ratio of base to curing agent of 1:1 was poured carefully onto the PDMS master after surface hydrophobic treatment, which was vacuumed for 5 min to eliminate bubbles and cured at 80°C for 4 h. Thus, the second replication was achieved. Finally, the synthesized PMVE/MA hydrogel (13 mL) in this study was poured into a holder where the Ecoflex master was fixed on the bottom. This holder was firstly placed in a vacuum oven (80°C) for 7 h to ensure that the mixture solution filled the microwells. Then, the

holder was transferred to an oven (90°C, 24 h). Consequently, the holder was placed in a fume hood and peeled off immediately. A pristine hydrogel microneedle patch was obtained and stored in a desiccator at 20°C when not in use.

For conductive MNs, the pristine MNs was firstly plasma-treated for 1 min. And 100 μL 0.5 mg/mL Cr dispersion solution in 0.1% chitosan was drop-casted on the surface of MNs immediately. And it was placed in oven (60°C, 30 min) to dry. Afterwards, a compact gold film was formed on its surface by Au spurring (10 mA, 600s). Then, a gold wire (diameter of 200 μm) was attached to the contact area of the MNs by brushing carbon paste (SPI Supplies Co., USA) and placed in the oven (60°C, 10 min). After, it was coated a gold film by Au spurring to maintain a consistent surface. Insulation and package step were applied for the contact and non-conductive area by Ecoflex (smooth-on 0030) precursor mixture at a weight ratio of base to curing agent of 1:1. Finally, it was placed in oven (60°C, 60 min). A conductive MNs was obtained. For reference MNs, the conductive MNs was pasted with Ag/AgCl ink (BAS Inc., Japan); for counter MNs, the conductive MNs was pasted with carbon paste (SPI Supplies Co., USA). Thus, a three-electrode MNs system was ready for subsequence modification and application. The morphology and thickness of the MNs was validated by a stylus profiler (AlphaStep D-600, KLA-Tencor Corp.).

4.3 Construction of CRISPR micro-electrode and CRISPR microneedles

For CRISPR micro-electrode construction, 0.2 mg/mL graphene dispersed (Sigma-Aldrich provided) in 0.1% chitosan was drop-casting on the surface and it was placed in oven (60°C, 10 min). And 10 μL 1-pyrenebutanoic acid (PBA, dissolved in N,N-Dimethylformamide, Aladdin Co., Shanghai) of 5 mM was drop-casted on this surface under 37°C for 1 h. PBA was stacked on the graphene surface via π-π interaction. And the micro-electrode was washed by ddH_2O. Accordingly[20,50], carboxyl group of PBA was activated by EDC (4 mM): NHS (11 mM) solution (100 μL:100 μL in 100 μL 50 mM 2-morpholinoethanesulfonic acid buffer, all provided by Aladdin Co., Shanghai) for 10 min. And the micro-electrode was incubated in 1 μM dCas9 (Tolo Biotechnology) for 30 min under 37°C. And 1% BSA blocked the non-specific active sites for 10 min under 37°C. It was washed by 2 mM $MgCl_2$. The micro-electrode was incubated in 1 μM sgRNA (Sangon Co., synthesized and provided) for 30 min under 37°C, and washed by 2 mM $MgCl_2$ for 1 min. Thus, a CRISPR micro-electrode was fabricated.

For CRISPR microneedles, before construction, the conductive MNs was sterilized under UV light for 10 min and plasma-treated for 1 min. 100 μL 0.2 mg/mL carboxyl graphene (XFNANO Co., Nanjing) dispersed in 0.1% chitosan was immediately drop-casted on MNs surface and placed in the oven for 30 min under 60°C. Accordingly[20,50], carboxyl group of graphene was activated by 100 μL mixed solution of EDC (4 mM): NHS (11 mM) with a volume of 200 μL:200 μL in 100 μL 50 mM 2-morpholinoethanesulfonic acid buffer (all provided by Aladdin Co., Shanghai) for 30 min under 37°C. The remainder solution on the MNs surface was eliminate by pipetting and placed in the oven to dry (40 min, 37°C). The MNs was incubated in 1 μM dCas9 (Tolo Biotechnology) for 30 min under 37°C and dried in

the oven (40 min, 37°C). 1% BSA blocked the non-specific active sites for 10 min under 37°C and dried in the oven (40 min, 37°C). The MNs was incubated in 1 μM sgRNA (Sangon Co., synthesized and provided) for 30 min under 37°C and washed by 2 mM $MgCl_2$ for 1 min. Finally, the MNs was dried in the oven (40 min, 37°C). A CRISPR MNs was obtained.

4.4 Iontophoretic wearable patch construction

Firstly, the crude PDMS precursor mixture at a weight of base to curing agent of 6g:0.6g was poured carefully onto the square plain petri dish master (diameter of 9 cm, Corning corporation) after surface hydrophobic treatment, which was vacuumed for 5 min to eliminate bubbles and cured at 80°C for 1h. The crude PDMS thin film was peeled from the substrate. Meanwhile, the 1% chitosan solution was prepared (1g chitosan in 100 mL of 2 % acetic acid, stirring for 5 h) and centrifugated (4000 rpm, 30 min) to eliminate bubble. Secondly, the prepared PDMS thin film was plasma-treated for 4 min. The 1% chitosan solution of 2 mL was immediately casted on the surface of the PDMS thin film. And it was curing in the oven (80°C, 1 h). Then, a chitosan modified PDMS thin film was obtained. A general microfluidic mask with the desired pattern was gently place on the surface of the modified thin film. A spray-gun (300 μm diameter, C100, Shibangde corporation, shanghai) spray-deposited the as-prepared CNT solution (XFNANO Co., Nanjing) to the modified PDMS surface through hollow region of the mask. The printed functional membrane was placed on a thermal plate to eliminate drops. Then, fabricated three-electrode microneedles were attached on the anode side of the thin film by 3M tape. Finally, a multifunctional wearable device was obtained. All the mechanical testing was performed on Instron 5966 electronic universal testing machine (Instron, USA)

4.5 Typical CRISPR, PCR and PAGE gel electrophoresis

A typical CRISPR reaction in a centrifugal tube was as follows. The pre-incubation solution comprised of 8.5 μL ddH_2O, 3 μL buffer, 1.5 μL sgRNA (20 μM), 1 μL spCas9 (1 μM, Tolo biotechnology), for 10 min, 25°C. Then, 6 μL EBV CfDNA PCR product was added for CRISPR reaction (incubated for 90 min under 37°C). Then, 1 μL Rnase A (5 mg/mL, Sangon Co., provided) was added to eliminate sgRNA for 30 min under 37°C. Finally, it was incubated in 95°C for 5 min to stop CRISPR as well as Rnase A reaction, releasing binding gene-edited EBV CfDNA[51,52].

Conserved nucleic acid fragments of the EBV BamHI-W region were screened (GenBank No. A10072.1) and cloned into the PUC57 plasmid, which was utilized as the standard containing the target nucleic acid fragment. All primers (Supplementary Table S2) used in the experiments were synthesized (Sangon Biotech Co., Ltd., Shanghai, China).

PCR was carried out using a Tiangen SuperReal Premix Plus Kit (Tiangen Biotech Co., Ltd., Beijing, China). The 50-μL PCR system comprised 25 μL of 2×SuperReal Premix plus, 1.5 μL of forward and reverse primers (final concentration of 400 nM), 2 μL of template, and 20 μL of RNase-free ddH_2O. The amplification was performed using a fluorescent quantitative PCR detection system (LineGene 9640,

Hangzhou Bioer Technology Co., Ltd., Hangzhou, China) according to the following two-step procedure: 1 cycle at 95°C for 15 min, followed by 40 cycles at 95°C for 10 s, 60°C for 20 s, and 72°C for 32 s.

For PAGE gel electrophoresis, the gel was comprised of 6 mL 30% Acryl/Bis solution, 5.634 mL ddH_2O, 240 μL 50×TAE buffer, 6 μL TMEMD. Samples and 6×ficoll gel loading buffer III were pre-mixed for 3 min, then added to the gel. Finally, standard PAGE gel electrophoresis (100 V, 110 min) was performed with an EPS 300 electrophoresis apparatus (Tanon, Shanghai). Afterwards, PAGE gel was stained in SYBR Green I (50 μL stock solution in 50 mL 1×TAE buffer) for 30 min and imaged by 4100 digital gel image processing system (Tanon, Shanghai).

All the primers used in the study are also listed in **Table S2**.

4.6 Electrochemical measurements

Differential pulse voltammetry (DPV) testing was conducted. The scanning potential range was set from − 0.2 V to 0.6 V at a scan rate of 50 mV/s in a 0.05 mM $K_3[Fe(CN)_6]/K_4[Fe(CN)_6]$ solution that contained 0.50 M KCl.

Cyclic voltammetry (CV) measurement was conducted for electrochemical characterization. The scanning potential range was set from − 0.2 V to 0.6 V at a scan rate of 50 mV/s in a 0.05 mol/L $K_3[Fe(CN)_6]/K_4[Fe(CN)_6]$ solution that contained 0.50 M KCl. Electrochemical impedance spectroscopy (EIS) was performed in the frequency range of 0.1 Hz to 100 000 Hz and at an alternating voltage of 5 mV. And i-t test was conducted with an initial potential of -0.1 V.

4.7 Animals experiments

Animals were cared for and maintained under the Guidelines of Laboratory Animals of Fudan University and approved by the Animal Ethics Committee of Fudan University, China (2021JSCHEM-020).

BALB/c nude female mice (aged 4 weeks) were purchased from Beijing Vital River Laboratory Animal Technology Co., Ltd. (Beijing, China). According to the reference, 500-μL volume of reprogramming CNE-Luc cells (2×10^6 cells/mL, 250μL) and BD matrigel (250 μL, Corning corporation) was subcutaneously injected into 8-week-old BALB/c nude mice[53,54]. The whole process was conducted at 4°C.

For bioluminescence, isofluorane anesthesia was maintained using a nose cone delivery system during image acquisition. Mice bearing with CNE-Luc cells and negative control mice were injected with 100 μL of D-Luciferin potassium salt (30 mg/mL, Shanghai Yeasen biotechnology Co., LTD). After 12 min, bioimaging signals was collected by CCD with exposure time of 60 s (in Vivo Xtreme, Bruker, USA).

Before real-time test, anaesthesia was applied to the mice (2 % avertin, 250 μL for each subject). 2 % avertin was prepared as followed: 0.625 g of 2,2,2-tribromoethanol (Sigma-Aldrich) was dissolved in 1.2 mL tert-amyl alcohol, and 30 mL ddH_2O was added. The solution was incubated in water-bath overnight (45°C) and protected by foil. Mouse skin was cleaned by scrub cream and disinfected by 75% ethanol on

a heating plate. Then, TE buffer was smeared on the region of interest close to anode side and dried by cotton. The conductive MNs was laminated on this region of interest. The work mode for animals consists of 1-min calibration, 3-min reverse iontophoresis, and 1-min biosensing signal collection.

4.8 Statistical analysis

All statistical results presented was performed by two-way ANOVA and linear regression analyzed by using origin 9.0 software. These results performed were mean ± SEM. Significance level was implied by *, **, ***, ****, ns for $p < 0.05$, $p < 0.01$, $p < 0.001$, $p < 0.0001$, no significance respectively.

References

1. Heikenfeld, J. et al. Accessing analytes in biofluids for peripheral biochemical monitoring. *Nat. Biotechnol.* **37**, 407–419 (2019).
2. Kim, J., Campbell, A. S., Ávila, B. E. F. D. & Wang, J. Wearable biosensors for healthcare monitoring. *Nat. Biotechnol.* **37**, 389–406 (2019).
3. Yang, Y. et al. A laser-engraved wearable sensor for sensitive detection of uric acid and tyrosine in sweat. *Nat. Biotechnol.* **38**, 217–224 (2020).
4. Shrivastava, S., Trung, T. Q. & Lee, N. E. Recent progress, challenges, and prospects of fully integrated mobile and wearable point-of-care testing systems for self-testing. *Chem. Soc. Rev.* **49**, 1812–1866 (2020).
5. Lee. G. H. et al. Multifunctional materials for implantable and wearable photonic healthcare devices. *Nat. Rev. Mater.* **5**, 149–165 (2020).
6. Bandodkar, A. J. et al. Sweat-activated biocompatible batteries for epidermal electronic and microfluidic systems. *Nat. Electron.* **3**, 554–562 (2020).
7. Sempionatto, J. R. et al. An epidermal patch for the simultaneous monitoring of haemodynamic and metabolic biomarkers. *Nat. Biomed. Eng.* https://doi.org/10.1038/s41551-021-00685-11-12 (2021).
8. Mishra, R. K. et al. Continuous opioid monitoring along with nerve agents on a wearable microneedle sensor array. *J. Am. Chem. Soc.* **142**, 5991–5995 (2020).
9. Samant, P. P. et al. Sampling interstitial fluid from human skin using a microneedle patch. *Sci. Transl. Med.* **12**, eaaw0285 (2020).
10. Zhu, J. et al. Gelatin methacryloyl microneedle patches for minimally invasive extraction of skin interstitial fluid. *Small* **16**, 1905910 (2020).
11. Yang, B., Fang, X. & Kong, J. In situ sampling and monitoring cell-free DNA of the Epstein-Barr virus from dermal interstitial fluid using wearable microneedle patches. *ACS Appl. Mater. Interfaces* **11**, 38448–38458 (2019).
12. Yang, B., Fang, X. & Kong, J. Engineered microneedles for interstitial fluid cell-free DNA capture and sensing using iontophoretic dual-extraction wearable patch. *Adv. Funct. Mater.* **30**, 2000591 (2020).

13. Anzalone, A. V., Koblan, L. W. & Liu, D. R. Genome editing with CRISPR-Cas nucleases, base editors, transposases and prime editors. *Nat. Biotechnol.* **38**, 824–844 (2020).
14. Ran, F. A. et al. Genome engineering using the CRISPR-Cas9 system. *Nat. Protoc.* **8**, 2281–2308 (2013).
15. Gootenberg, J. S. et al. Multiplexed and portable nucleic acid detection platform with Cas13, Cas12a, and Csm6. *Science* **360**, 439–444 (2018).
16. Myhrvold, C. et al. Field-deployable viral diagnostics using CRISPR-Cas13. *Science* **360**, 444–448 (2018).
17. Chen, J. S. et al. CRISPR-Cas12a target binding unleashes indiscriminate single-stranded DNase activity. *Science* **360**, 436–439 (2018).
18. Bruch, R. et al. CRISPR/Cas13a-powered electrochemical microfluidic biosensor for nucleic acid amplification-free miRNA diagnostics. *Adv. Mater.* **31**, 1905311 (2019).
19. Dai, Y. et al. Exploring the trans-cleavage activity of CRISPR-Cas12a (cpf1) for the development of a universal electrochemical biosensor. *Angew. Chem. Int. Ed.* **58**, 17399–17405 (2019).
20. Hajian, R. et al. Detection of unamplified target genes via CRISPR-Cas9 immobilized on a graphene field-effect transistor. *Nat. Biomed. Eng.* **3**, 427–437 (2019).
21. Fozouni, P. et al. Amplification-free detection of SARS-CoV-2 with CRISPR-Cas13a and mobile phone microscopy. *Cell* **184**, 323–333 (2021).
22. Chan, K. C. A. et al. Analysis of plasma Epstein–Barr virus DNA to screen for nasopharyngeal cancer. *N. Engl. J. Med.* **377**, 513–522 (2017).
23. Young, L. S., Yap, L. F. & Murray, P. G. Epstein–Barr virus: more than 50 years old and still providing surprises. *Nat. Rev. Cancer*, **16**, 789 (2016).
24. Qi, D. Zhang, K. Tian, G. Jiang, B. & Huang, Y. Stretchable electronics based on PDMS substrates. *Adv. Mater.* **33**, 2003155 (2021).
25. Mekler, V., Minakhin, L. & Severinov, K. Mechanism of duplex DNA destabilization by RNA-guided Cas9 nuclease during target interrogation. *Proc. Natl. Acad. Sci. U. S. A.* **114**, 5443–5448 (2017).
26. Cong, L. et al. Multiplex genome engineering using CRISPR/Cas systems. *Science* **339**, 819–823 (2013).
27. Nishimasu, H. et al. Crystal structure of Cas9 in complex with guide RNA and target DNA. *Cell* **156**, 935–949 (2014).
28. Bergveld, P. A critical evaluation of direct electrical protein detection methods. *Biosens. Bioelectron.* **6**, 55–72 (1991).
29. Hsieh, K., Patterson, A. S., Ferguson, B. S., Plaxco, K. W., Soh, H. T. Rapid, sensitive, and quantitative detection of pathogenic DNA at the point of care through microfluidic electrochemical quantitative loop-mediated isothermal amplification *Angew. Chem. Int. Ed.* **51**, 4896–4900 (2012).
30. Schmittgen, T. D. & Livak, K. J. Analyzing real-time PCR data by the comparative CT method. *Nat. Protoc.* **3**, 1101 (2008).

31. Kusama, S. et al. Transdermal electroosmotic flow generated by a porous microneedle array patch. *Nat. Commun.* **12**, 658 (2021).
32. Yu, H. et al. Fabrication of aptamer-modified paper electrochemical devices for on-site biosensing. *Angew. Chem.* **133**, 3030–3037 (2021).
33. Fu, H. et al. Morphable 3D mesostructures and microelectronic devices by multistable buckling mechanics. *Nat. Mater.* **17**, 268–276 (2018).
34. Amjadi, M., Yoon, Y. J. & Park, I. Ultra-stretchable and skin-mountable strain sensors using carbon nanotubes–Ecoflex nanocomposites. *Nanotechnology* **26**, 375501 (2015).
35. Wang, C. et al. Advanced carbon for flexible and wearable electronics. *Adv. Mater.* **31**, 1801072 (2019).
36. Liu, Z. et al. Thickness-gradient films for high gauge factor stretchable strain sensors. *Adv. Mater.* **27**, 6230–6237 (2015).
37. Lu, N., Lu, C., Yang, S. & Rogers, J. Highly sensitive skin-mountable strain gauges based entirely on elastomers. *Adv. Funct. Mater.* **22**, 4044–4050 (2012).
38. Civalek, Ö. & Demir, Ç. Bending analysis of microtubules using nonlocal Euler-Bernoulli beam theory. *Appl. Math. Model.* **35**, 2053–2067 (2011).
39. Wang, Y. et al. A durable nanomesh on-skin strain gauge for natural skin motion monitoring with minimum mechanical constraints. *Sci. Adv.* **6**, eabb7043 (2020).
40. Kim, H. J., Sim, K., Thukral, A. & Yu, C. Rubbery electronics and sensors from intrinsically stretchable elastomeric composites of semiconductors and conductors. *Sci. Adv.* **3**, e1701114 (2017).
41. Oh, J. Y.et al. Stretchable self-healable semiconducting polymer film for active-matrix strain-sensing array. *Sci. Adv.* **5**, eaav3097 (2019).
42. Jang, H. et al. Graphene-based flexible and stretchable electronics. *Adv. Mater.* **28**, 4184–4202 (2016).
43. Knight, S. C. et al. Dynamics of CRISPR-Cas9 genome interrogation in living cells. *Science* **350**, 823–826 (2015).
44. Xiong, Y. et al. Functional DNA regulated CRISPR-Cas12a sensors for point-of-care diagnostics of non-nucleic-acid targets. *J. Am. Chem. Soc.* **142**, 207–213 (2019).
45. Kim,H. et al. Clustered Regularly Interspaced Short Palindromic Repeats-Mediated Surface-Enhanced Raman Scattering Assay for Multidrug-Resistant Bacteria. *ACS Nano* **14**, 17241–17253 (2020).
46. Yuan, C. et al. Universal and naked-eye gene detection platform based on the clustered regularly interspaced short palindromic repeats/Cas12a/13a system. *Anal. Chem.* **92**, 4029–4037 (2020).
47. Hu, J., Jiang, M., Liu, R. & Lv, Y. Label-free CRISPR/Cas9 assay for site-specific nucleic acid detection. *Anal. Chem.* **91**, 10870–10878 (2019).
48. Xu, W., Jin, T., Dai, Y. & Liu, C. C. Surpassing the detection limit and accuracy of the electrochemical DNA sensor through the application of CRISPR Cas systems. *Biosens. Bioelectron.* **155**, 112100 (2020).

49. Tierney, M. J. et al. The GlucoWatch® biographer: a frequent, automatic and noninvasive glucose monitor. *Ann. Med.* **32**, 632–641 (2000).
50. Yu, X. et al. Surface-adaptive and initiator-loaded graphene as a light-induced generator with free radicals for drug-resistant bacteria eradication. *ACS Appl. Mater. Interfaces* **12**, 52229 (2020).
51. Ma, H. et al. CRISPR-Cas9 nuclear dynamics and target recognition in living cells. J. Cell Biol. **214**, 529–537 (2016).
52. Wang, X. et al. Clustered regularly interspaced short palindromic repeats/Cas9-mediated lateral flow nucleic acid assay. *ACS Nano* **14**, 2497–2508 (2020).
53. Fahmy, R. G., Dass, C. R., Sun, L. Q., Chesterman, C. N. & Khachigian, L. M. Transcription factor Egr-1 supports FGF-dependent angiogenesis during neovascularization and tumor growth. *Nat. Med.* **9**, 1026–1032 (2003).
54. Dai, L. et al. SARI inhibits angiogenesis and tumour growth of human colon cancer through directly targeting ceruloplasmin. *Nat. Commun.* **7**, 11996 (2016).

Declarations

Acknowledgements

This work was supported by the National Natural Science Foundation of China (21974028 and 21427806), China National Postdoctoral Program for Innovative Talents (BX20200090), and Shanghai Post-doctoral Excellence Program (2020066).

Author contributions

B.Y. and X.F. conceived the idea of the hydrogel microneedles and wearable. B.Y. designed wearable patch and bio-microfluidics and animal experiments. B.Y. synthesized hydrogel. B.Y. conducted electrochemical, bio-microfluidics, animal experiments, and. B.Y. and X.F. applied the microneedles combined with wearable device for animals and analyzed the data from *in vitro* and *in vivo* tests. B.Y. and X.F. wrote the manuscript. X.F. and J.K. supervised the study.

Competing interests

The authors declare no competing financial interest.

Figures

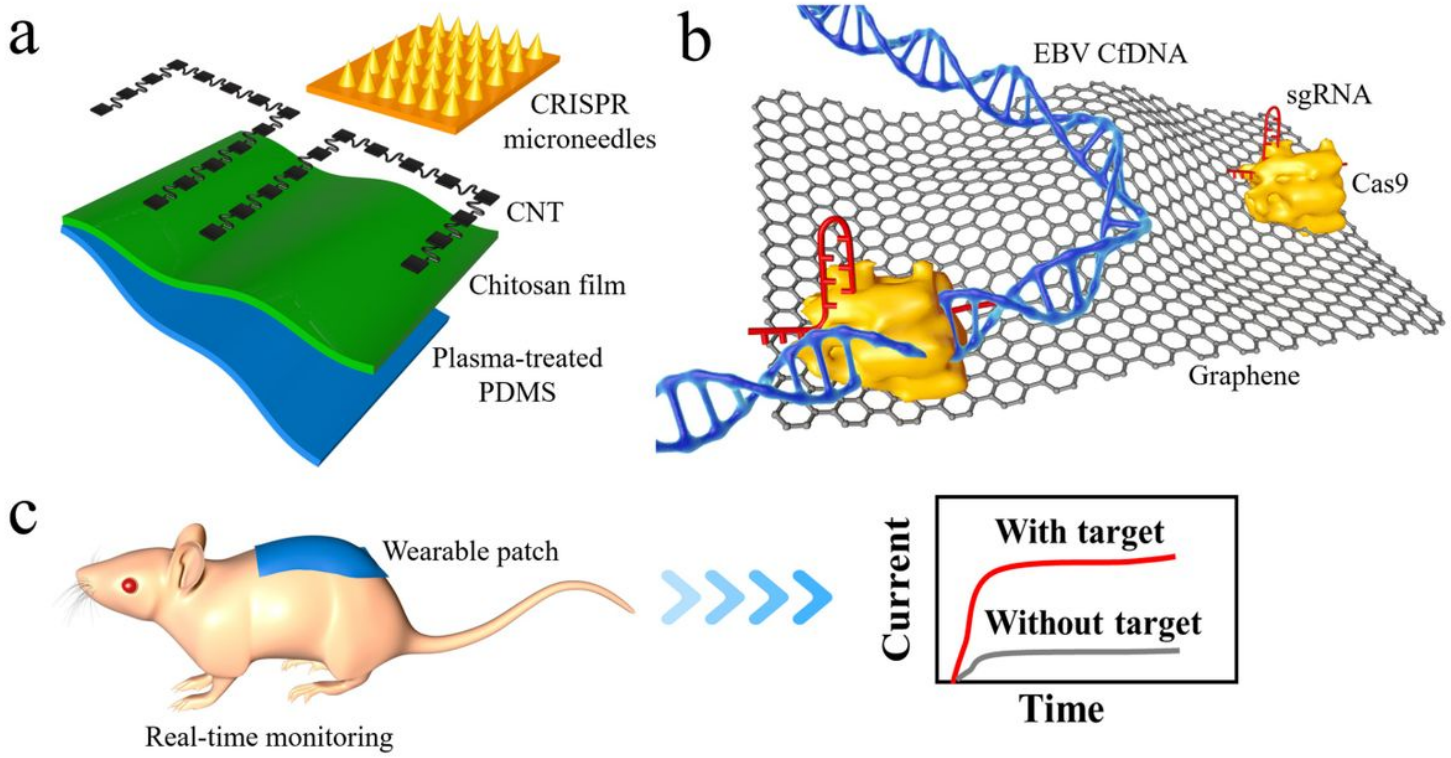

Figure 1

Schematics of CRISPR-Cas9 activated graphene biointerfaces for extraction and real-time in vivo monitoring of EBV CfDNA in ISF. (a) Workflow of the wearable patch fabrication. (b) Scheme showing CRISPR microneedles integrated with the dCas9 enzyme and a sequence-specific sgRNA (denoted as dRNP) immobilized on a carboxyl graphene surface. (c) Real-time monitoring of the enriched EBV CfDNA based on reverse iontophoresis and CRISPR-Cas9 activated graphene biointerfaces. The specific recognition of EBV CfDNA to dRNP regulates the electrochemical characteristics and potential difference of the graphene layer, generating electrical signal output.

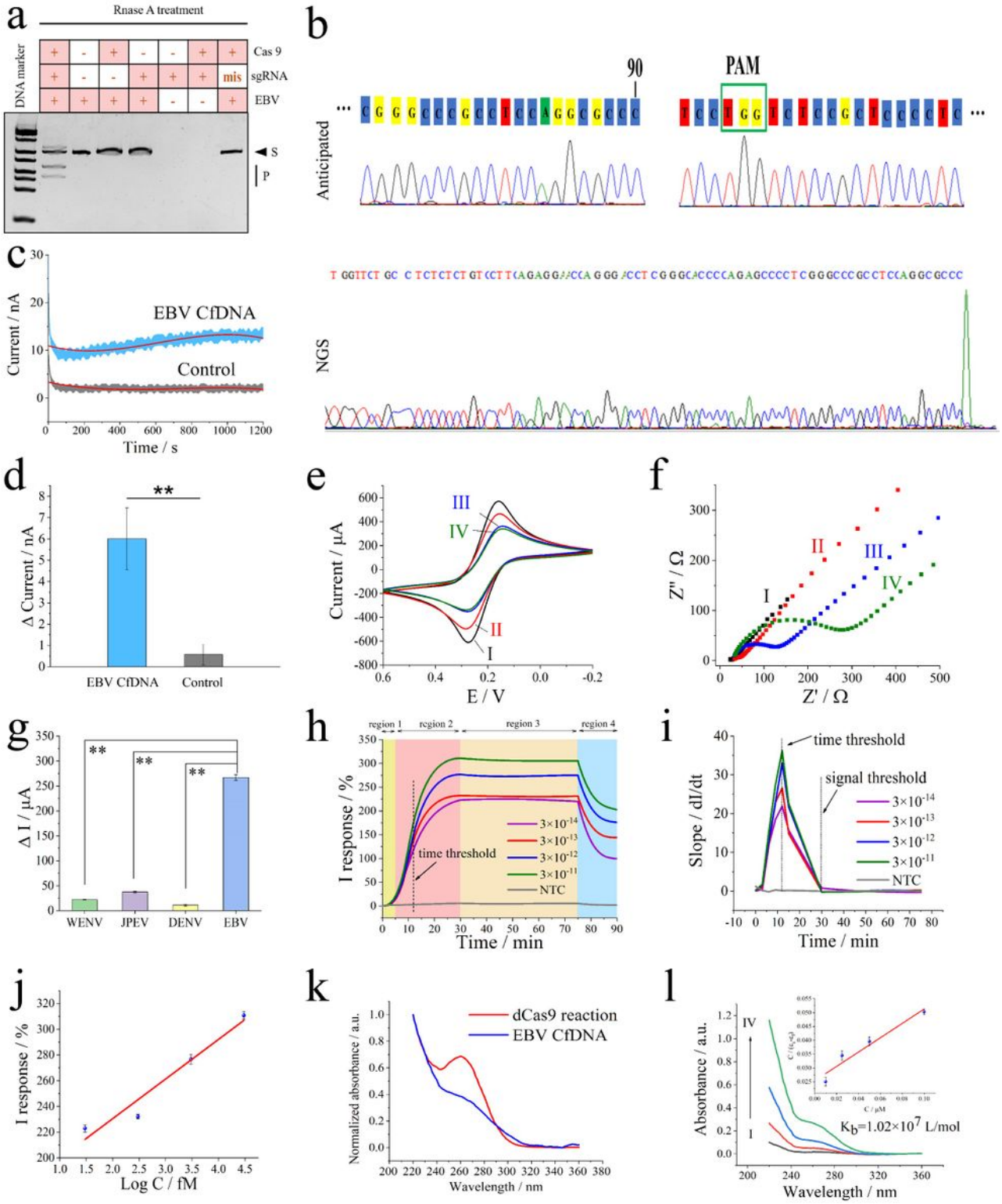

Figure 2

Validation of the CRISPR system and off-wearable strategy targeting EBV CfDNA on a solid commercial microelectrode. (a) In vitro cleavage ability of dRNP validated by PAGE. Each sample was incubated at 37 °C for 90 min before loading on a PAGE gel (100 V, 110 min, 1× TAE buffer) and then stained with SYBR green I for 30 min prior to gel imaging, where S and P refer to the sample and product, respectively. (b) Next-generation sequencing of CRISPR-Cas9 gene editing in EBV CfDNA. (c) CRISPR-Cas9 system

representative real-time i-t curve raw data for detecting EBV CfDNA targets (sample interval 0.1 s, sampling time 1200 s); the red line represents the fitting curve (polynomial order=3). (d) The current signal output of the CRISPR-Cas9 system in the presence of EBV CfDNA, analyzed by two-way ANOVA, n=3. (e) CV plots and (f) EIS spectra of the microelectrode under different conditions. I, II, III and IV refer to the bare microelectrode, graphene-modified microelectrode, CRISPR microelectrode and CRISPR microelectrode targeting 2×10-10 M EBV CfDNA, respectively. (g) Specificity of the CRISPR-based microelectrode; 100 interferences showed a slight influence, 0.05 M [Fe(CN)6]3−/4− as the probe (error bars, mean±SEM, n=3). (h) Real-time CRISPR-based microelectrode I response targeting variable concentrations of EBV CfDNA. Regions 1, 2, 3 and 4 refer to the phase before the time threshold, the phase after the time threshold, the stable period, and the rinsing step, respectively. (i) Slope of the plots from figure 2h. (j) Calibration curve of the real-time I response from Figure 2h (error bars, mean±SEM, n=3). (k) The interaction of dRNP and EBV CfDNA. (l) UV-vis absorption changes; inset: calibration curve, dRNP with EBV CfDNA; I, II, III, and IV: R0.1, R0.25, R0.5, and R1.0, respectively.

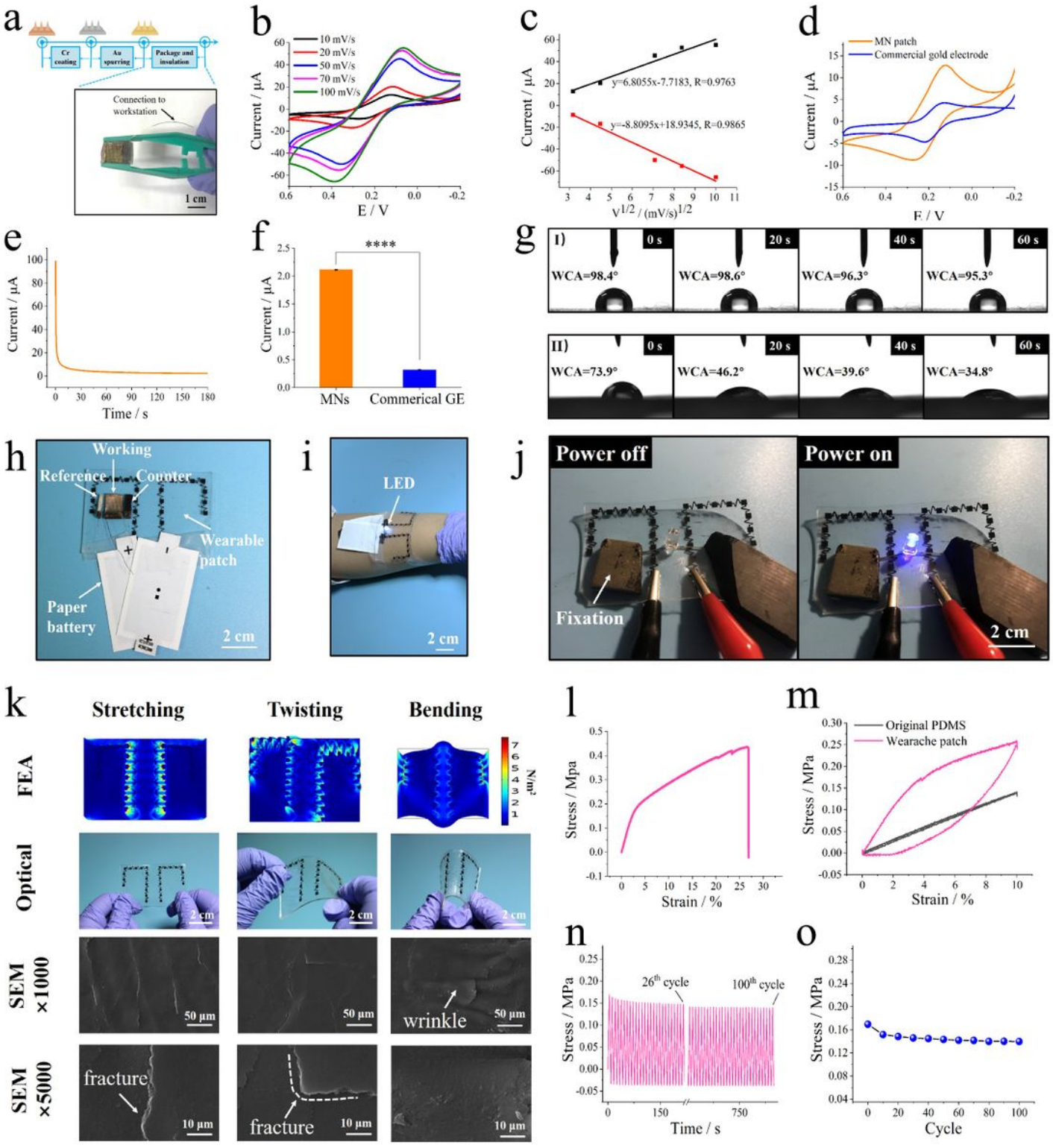

Figure 3

Fabrication, electrochemical and mechanical properties of the CRISPR wearable patch. (a) Schematic illustration of the conductive MNs. (b) CV plots of the as-fabricated conductive MNs under different scanning rates. (c) The relationship between the square root of the scanning rate and the corresponding peak current using a 1 mM [Fe(CN)6]3−/4− probe. (d) CV plots of the conductive MNs and commercial gold electrode using a 1 mM [Fe(CN)6]3−/4− probe. (e) Real-time i-t curve recorded by the conductive

MNs in PBS buffer (0.01 M, pH 7.4). (f) The real-time current of the conductive MNs and commercial gold electrode in PBS buffer (0.01 M, pH 7.4). (g) Contact angle testing of water droplets on the surface of the I) original PDMS film and II) hydrophilic-treated PDMS film. (h) Photograph of the CRISPR wearable patch based on reverse iontophoresis and three-electrode MNs. (i) The printed wearable patch mounted on skin. (j) A blue LED powered by the wearable patch with a voltage of 6 V. (k) Finite elemental analysis, optical photographs and SEM of the wearable device under different mechanical distortions, including stretching, twisting and bending. (l) Strain versus stress curve for the wearable patch, n=3. (m) A single stretch-release cycle with 10% strain for two different membranes, n=3. (n) Stress variation of the wearable patch in a 100-cycle test with a strain of 4%. (o) Stress changes of the wearable patch every ten cycles.

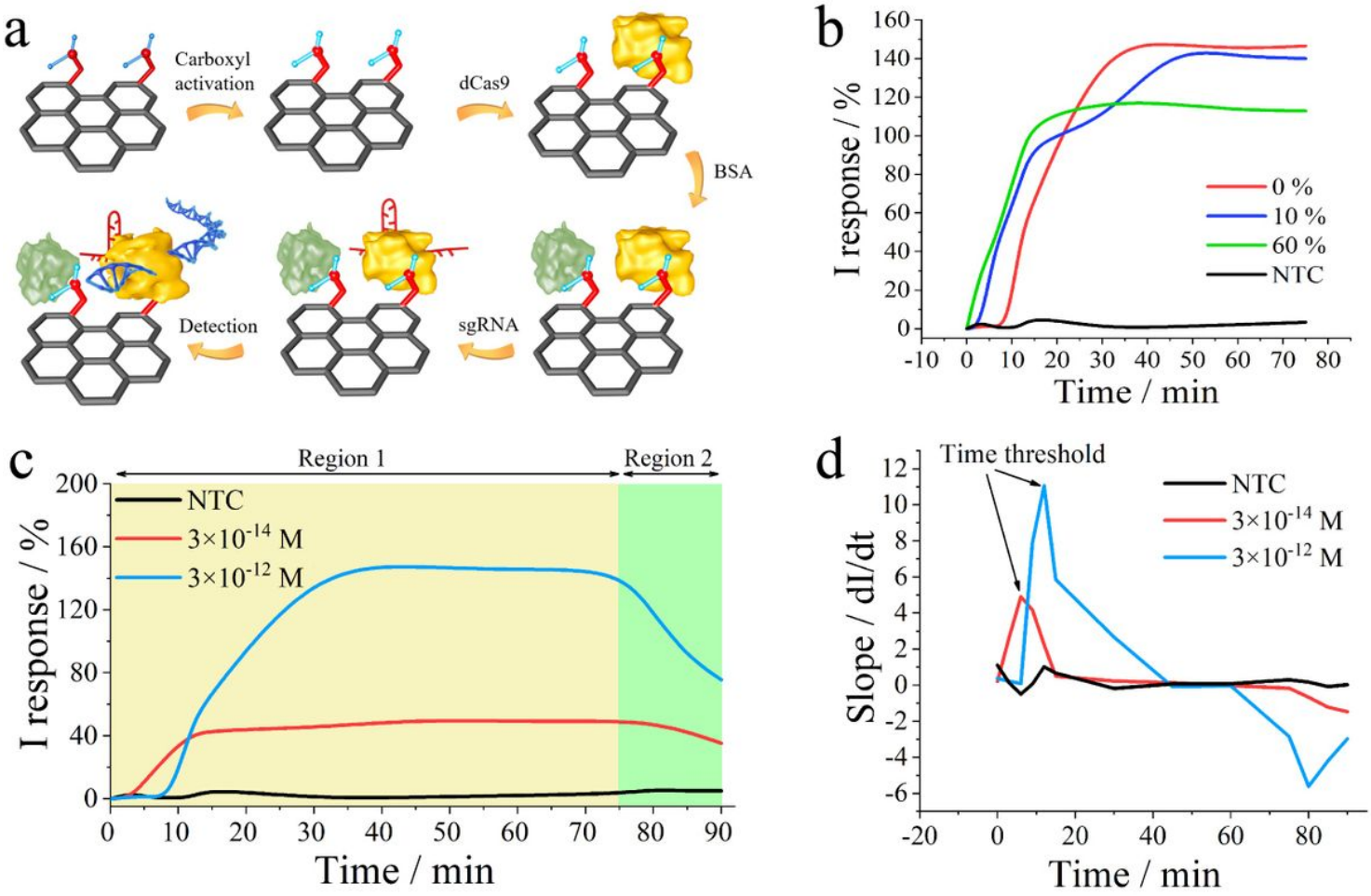

Figure 4

Analytical performance of CRISPR MNs targeting EBV CfDNA in vitro. (a) Schematic of CRISPR MN preparation. The as-fabricated conductive MNs were first sterilized by UV light. A carboxyl graphene/chitosan solution was drop-cast on the MN surface at 60 °C for 30 min. Carboxyl graphene was activated via EDC/NHS (highlighted in radiance). The terminal carboxyl groups of graphene acted as tethering units to covalently bind with dCas9. Then, those nonspecific binding sites were blocked with 1% BSA. sgRNA complementary to a DNA of interest was introduced through the binding of tracrRNA and dCas9. Finally, the prepared CRISPR MNs were stored at -20 °C when not used. (b) Anti-interference ability of the CRISPR MNs for 3×10-12 M EBV CfDNA in the presence of various concentrations of fetal bovine

serum, n=3. (c) Real-time CRISPR MNs I response targeting variable concentrations of EBV CfDNA; regions 1 and 2 refer to real-time steps and rinse steps, respectively. n=3. (d) Slope of the plots from Figure 4c.

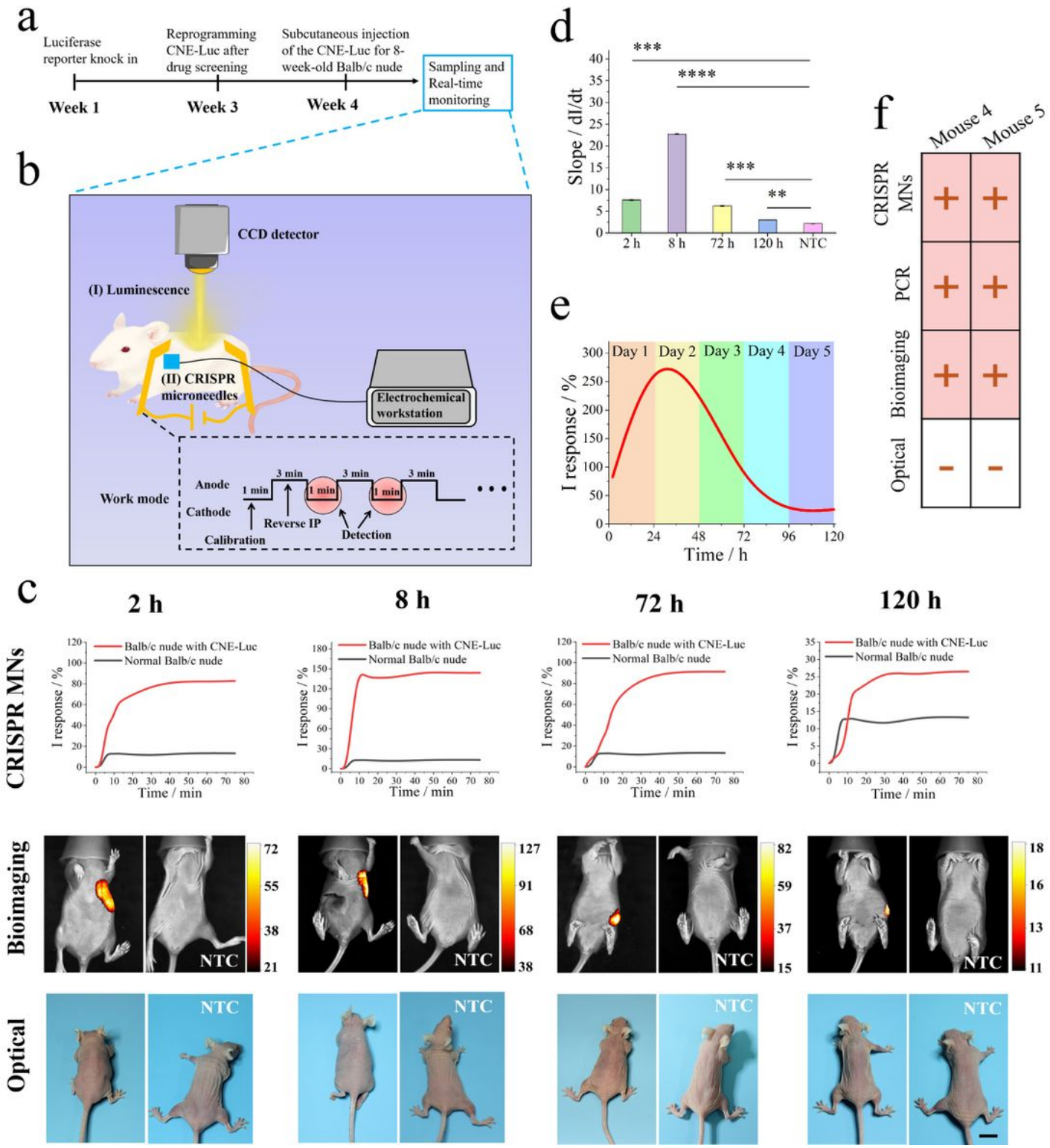

Figure 5

Demonstration of the CRISPR MN wearable system in mice. (a) Timeline of real-time monitoring in CNE-Luc-bearing mice. (b) Schematic illustration of in vivo real-time sampling and monitoring, including (I)

chemiluminescence bioimaging and (II) CRISPR MNs for tumor-bearing mice. The CRISPR MN system was calibrated in PBS (37 °C, 0.01 M, pH 7.4) for 1 min to eliminate sensor-to-sensor variation in electrical output. The red circle represented the detection timepoint. The skin stratum corneum of all BALB/c nude mice was cleaned by scrub cream, disinfection with 75% ethanol, and smearing with 100 μL TE buffer (pH 8.0). The region of interest on mouse skin was dried with cotton. Finally, the mice were placed on a heat plate during the real-time monitoring procedures. (c) Parallel trials on mice at different time points, scale bar: 1 cm. (d) Slope of the plot from BALB/c nude mice real-time detection, *p<0.05, **p<0.01, ***p<0.001, ****p<0.0001, and ns referring to no significant difference, as analyzed by two-way ANOVA. (e) In vivo dynamic change in EBV CfDNA levels in BALB/c nude mice detected by the CRISPR MN system during the first five days. (f) Four independent methods applied to 18-day CNE-Luc-bearing BALB/c nude mice demonstrated that the CRISPR MN wearable system was as accurate as the gold-standard PCR (blood sampling by a commercial kit) in terms of qualitative analysis.

Supplementary Files

This is a list of supplementary files associated with this preprint. Click to download.

- MovieS1.mp4
- MovieS2.mp4
- SupplementaryInformation.docx